Applied Catalysis B: Environmental 256 (2019) 117817

Contents lists available at ScienceDirect

Applied Catalysis B: Environmental

journal homepage: www.elsevier.com/locate/apcatb

Engineering highly active oxygen sites in perovskite oxides for stable and efficient oxygen evolution

Jie Xiong[a,e,1], Hong Zhong[c,1], Jing Li[a,1], Xinlei Zhang[a], Jiawei Shi[a], Weiwei Cai[a,*], Konggang Qu[b], Chengzhou Zhu[d,*], Zehui Yang[a,*], Scott P. Beckman[c], Hansong Cheng[a]

[a] Sustainable Energy Laboratory, Faculty of Materials Science and Chemistry, China University of Geoscinces, Wuhan, 430074, China
[b] School of Chemistry and Chemical Engineering, Liaocheng University, Liaocheng, 252059, China
[c] School of Mechanical and Materials Engineering, Washington State University, Pullman, WA 99164, United States
[d] Key Laboratory of Pesticide and Chemical Biology Ministry of Education, College of Chemistry, Central China Normal University, Wuhan 430079, China
[e] College of Chemistry, Chemical Engineering and Materials Science, Zaozhuang University, Zaozhuang, 277160, China

ARTICLE INFO

Keywords:
Oxygen evolution reaction
Perovskite oxide catalyst
$Ba_{0.5}Sr_{0.5}Co_{0.8}Fe_{0.2}O_{3-\delta}$
F substitution
Highly active oxygen site

ABSTRACT

Perovskite oxides, represented by $Ba_{0.5}Sr_{0.5}Co_{0.8}Fe_{0.2}O_{3-\delta}$ (BSCF), with O anion partially substituted by F anion are designed. Introduction of F in perovskite lattice initiated the transition of Co(III) and Fe(III) species to lower oxidation states and triggered the surface O anion to be activated to highly oxidative O^{2-}/O^{-}, which is deemed to be efficient active sites for oxygen evolution reaction (OER) catalysis. As a consequence, the F substituted BSCF (F-BSCF) catalyst exhibits outstanding electrocatalytic activity with overpotential of only 280 mV to deliver 10 mA cm^{-2} OER, which is among the results for state-of-the-art metal oxide based catalysts. Strikingly, an stable chronoamperometric response prolonged for 100 h and an impressive cycling stability demonstrate its prominent durability, much superior to the commercial IrO_2 catalyst. These findings highlight the promising potential of F substitution as an efficient strategy for active site engineering in traditional precious metal-free OER electrocatalysts.

1. Introduction

Hydrogen energy technology has been considered as one of the most promising renewable energy sources to replace the fossil fuels [1–3]. As the key segment to accomplish the hydrogen energy cycling, hydrogen generation from water splitting driven by electricity is still hindered by the noble-metal catalyst dependence of hydrogen evolution reaction (HER) [4–7] and oxygen evolution reaction (OER) [8–14]. The state-of-the-art OER catalyst is IrO_2, which can provide continuous formation of surface oxygen binding intermediates during the OER process [15,16]. Due to the naturally sluggish kinetics and multistep electron transfer reaction pathways, cost-effective metal oxides were extensively studied for superior OER catalytic performance [17–22] and reduced cost. By engineering oxygen defects [23–26] or regulating the cations [27–29], OER activity of the metal oxide based catalysts can be boosted by virtue of the altered surface electronic state. However, oxygen defects engineered by the traditional strategies including engraving, reduction and annealing may not be stable during the electrochemical oxidation circumstances [30]. Other than these traditional strategies, oxygen defects in the ABO_3-type perovskite oxides can be facilely engineered by adjusting the metal cations in either A or B sites [31–33]. $Ba_{0.5}Sr_{0.5}Co_{0.8}Fe_{0.2}O_{3-\delta}$ (BSCF) was experimentally proved to be one of the most effective perovskite OER catalysts due to the fact that the surface cation e_g electron occupancy of surface transition metal ions, suggested as the OER activity descriptor [31,34], is very close to unity. To further improve the OER catalytic activity of the perovskite oxides, represented by BSCF, extra active sites have been therefore engineered *via* utilization of functionalized carbon support [35,36] or above-mentioned traditional reduction [37,38].

Here in this work, a facile fluorine doping strategy was proposed to engineer extra oxygen-active sites in BSCF, for stable and efficient OER catalysis, inspired by the fact that F anion in the oxyfluoride could dramatically enhance the surface exchange and chemical bulk diffusion properties [39,40], improve the lattice oxygen mobility [41] as well as optimize the O *p*-band center and activate the lattice oxygen [42]. As demonstrated in Fig. 1a, O^{2-} is partially substituted by the F^{-} to form M···F···M (M = Co or Fe) coordination ligand in the presence of F source during BSCF sythesis. It incurs the valence-sensitive Co(III), Fe(III)

* Corresponding authors.
E-mail addresses: willcai1985@gmail.com (W. Cai), czzhu@mail.ccnu.edu.cn (C. Zhu), yeungzehui@gmail.com (Z. Yang).
[1] These authors contributed equally.

https://doi.org/10.1016/j.apcatb.2019.117817
Received 19 January 2019; Received in revised form 26 May 2019; Accepted 3 June 2019
Available online 16 June 2019

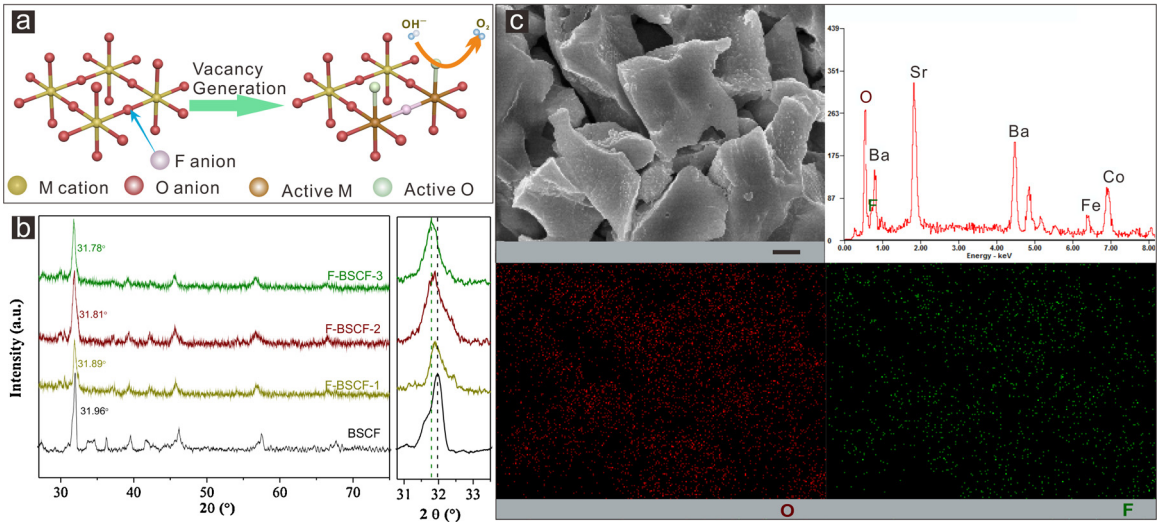

Fig. 1. F doping in BSCF. (a) Process of the highly oxidative active O engineering by F substitution in BSCF; (b) XRD spectra of the F-BSCF-*x* catalysts and the pristine BSCF catalyst; (c) SEM image and corresponding EDS spectrum, elemental mappings of the F-BSCF-2 catalyst (scale bar: 0.5 μm).

species to be reduced to Co(II) and Fe(II) (active M), respectively, and concurrently induces the surface O anion to be activated to engender highly oxidative O^{2-}/O^{-} specie due to the easier fromation of bulk oxygen vacancy resulted from charge compensation when F^{-} substitutes for O^{2-} according to the density functional theory (DFT) calculations. The O^{2-}/O^{-} specie (active O) can be considered as highly catalytic reactive sites [9,18] for efficient OER catalysis. As a result, OER activity on BSCF can be significantly improved by more than 150% due to the facilely engineered stable and active O^{2-}/O^{-}species on BSCF surface, which was confirmed by the systematic physical characterizations, and almost no activity decay was detected during the 3000-cycles stability test and 100 h durability test.

2. Results and discussion

The successful synthesis of BSCF and the F substituted BSCF (F-BSCF) catalysts with various F contents can be confirmed by the X-ray diffraction (XRD) patterns in Fig. 1b [35]. All the characteristic peaks of BSCF can be detected in the XRD patterns of F-BSCF catalysts and pristine BSCF [35,43]. More importantly, the diffraction peaks in the spectra of F-BSCF-*x*, where *x* is the designed F amount of fluorine source (in mmol), are slightly negatively shifted. The (110) peak of F-BSCF-3 is negatively shifted from 2θ = 31.96° of the pristine BSCF to 2θ = 31.78°. The negative shifting of the XRD spectrum is ascribed to the slightly expanded lattice due to the F anion substituting in the BSCF lattice. It would initiate the reduction of valence alterable B-site cations other than the oxide state invariable A-site cations [35] for the sake of charge compensation. The valence negative-shifted metal cation possesses a larger ionic radius than its more positive cation counterpart, which leads to the distance between two neighbored M cations being enlarged. Successful doping of F in the F-BSCF catalysts can also be directly confirmed by the energy dispersive spectrometry (EDS) elemental mapping on corresponding scanning electron microscope (SEM) images (Fig. 1c and Fig. S1). F is found to be uniformly distributed with O in the F-BSCF catalysts.

The state of F anions in the F-BSCF catalysts was further revealed by Fourier transform infrared spectroscopy (FT-IR) spectra (Fig. S2). For the pristine BSCF, a characteristic absorption band at ca. 580 cm^{-1} is attributed to Co-O stretching vibration in the perovskite-type structure [44,45]. Maintenance of the perovskite structure in the F-BSCF catalysts can be also confirmed by the absorption resonance around 580 cm^{-1} in the FT-IR spectra [45]. With the F doping, characteristic absorption band appeared at ca. 750 cm^{-1} is attributed to the stretching of M—F bond [46], indicating that F anions in the F-BSCF catalysts interact with B type cations in the ABO_3 perovskite-type structure.

The partial substitution of O^{2-} by F^{-} provides the possibility of creating oxidative O^{2-}/O^{-} species in view of charge compensation, which is expected to be active for OER. OER catalytic activity of the F-BSCF catalysts was then investigated with the linear sweep voltammetry (LSV) curves compared in Fig. 2a. Similar to the previous literature [47], BSCF performs better than the commercial IrO_2 catalyst with the overpotential at 10 mA cm^{-2} (η_{10}) decreased by ca. 10 mV. As expected, F-BSCF-1 with 1% F atomic ratio exhibited significantly enhanced OER activity compared with the pristine BSCF. η_{10} of F-BSCF-1 is low to 302 mV, more than 40 mV lower compared with the pristine BSCF. Further increasing the F content, F-BSFC-2 exhibited the greatest OER catalytic activity among the three prepared F-BSFC catalysts. η_{10} of F-BSCF-2 is further decreased to 280 mV, which is among the best metal oxide OER catalysts (Table S3) [17,48–54]. The enhanced OER performance of F-BSCF catalysts are in keeping with the promoted kinetic metrics with the lower Tafel slopes than that of IrO_2 (inset of Fig. 2a). With the current density elevated, which is more practical in the real electrolysis devices, the advantage of the F-BSCF catalysts is even more remarkable. OER potential on F-BSCF-2 was measured to be 1.60 V to achieve an anodic current density of 50 mA cm^{-2} (η_{50}), which is 75 mV lower than that on BSCF. In order to straightforwardly evaluate the OER catalytic activity on different catalysts, current densities at 1.63 V (400 mV overpotential) were compared in Fig. 2b. OER current density on the F-BSCF-2 catalyst is 68 mA cm^{-2}, ca. 3.5 times as high as that on the IrO_2, indicating a 2.5 times higher OER catalytic activity of the F-BSCF-2 compared with IrO_2. Further increase the F content would decay the OER catalytic activity. η_{10} of F-BSCF-3 was significantly increased to 328 mV. This decrement on OER activity is attributed to the digestion of the highly oxidative active O^{2-}/O^{-} species by extra F (Fig. 2c). The M—O—M bond would be replaced by two M—F bonds in this case and no B-site cation reduction as well as highly oxidative O^{2-}/O^{-} species was actually engineered by F doping.

DFT calculations were therefore performed to investigate the influence of F substitution on formation of bulk oxygen vacancies, which is strongly related to the surface O^{2-}/O^{-} species generation. (Details in Supporting Information) With proper F substitution, the vacancy formation energies can be reduced (Table S1), the covalent bonds of O with these Co and Fe atoms can be weakened (Table S2). The electronic structures of BSCF models before and after F substitution were further studied in order to investigate the influence of F substitution on M–O hybridization in BSCF. The projected density of states (PDOS) on metal

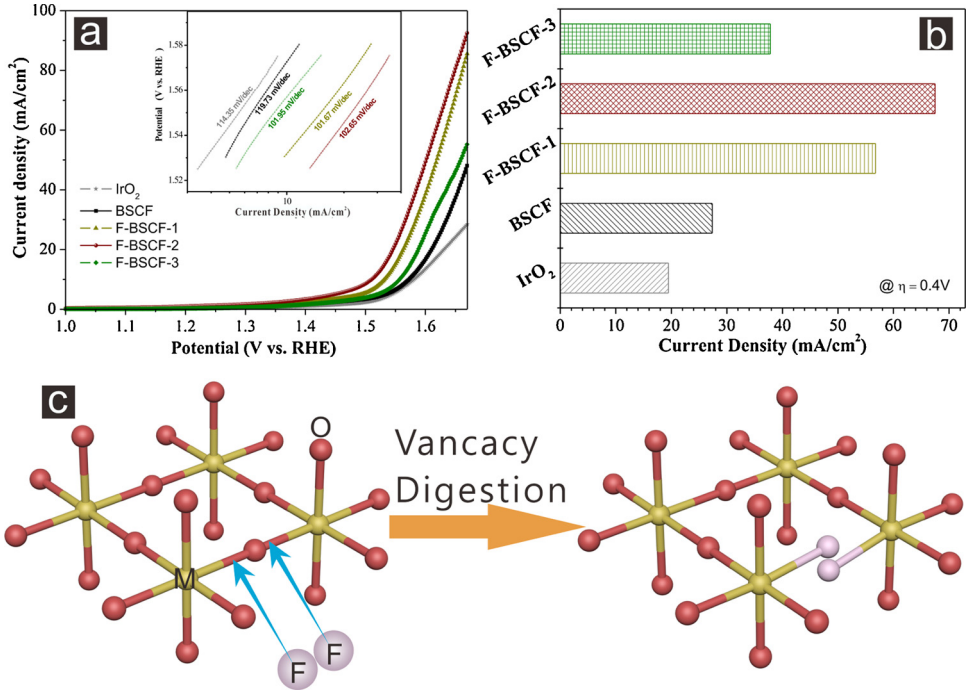

Fig. 2. OER activity. (a) LSV curves (inset: Tafel plots) and (b) specific current density at 1.63 V vs. RHE of OER on the F-BSCF, pristine BSCF and the commercial IrO_2 catalysts; (c) Schematic diagram of the digestion process of highly oxidative active oxygen in the F-BSCF-3 catalyst.

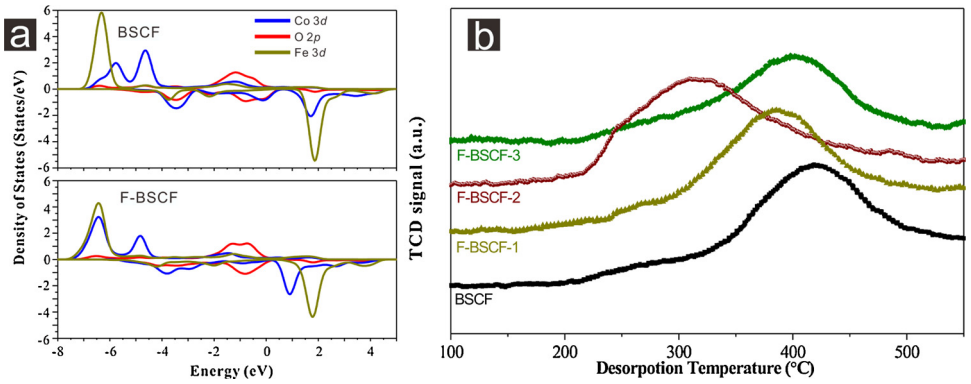

Fig. 3. (a) Projected density of states (PDOS) of Co 3*d*, O 2*p* and Fe 3*d* orbits in BSCF and F-BSCF. (The Fermi levels are set to 0 eV and the O14 (labelled in Scheme S1) in BSCF model is substituted by a fluorine atom in the F-BSCF model. (b) TPD profiles of the F-BSCF and pristine BSCF catalysts.

3*d* and oxygen 2*p* states of BSCF model and F-BSCF model, in which the O14 (labelled in Scheme S1) in BSCF model is substituted by F, are shown in Fig. 3a. After F substituting, the resonance peaks between O 2*p* and M (Fe and Co) 3*d* (−6.5 eV, −4.5 eV and −2.1 eV for O-Fe and −3.4 eV, −1.0 eV and −0.1 eV for O-Co) either disappear or weaken, suggesting a weakened M—O hybridization and therefore, weaker bonding interactions between O and M in BSCF. Thus, the formation of oxygen vacancy at O19 site (labelled in Scheme S1) in F-BSCF model is more energetically favorable than that in BSCF model. However, excess F atoms lead to an increased energy to form oxygen vacancies due to the extra F substituting to the sites that increase the vacancy formation energy (Table S1). This aggrees well with the activity decay of F-BSCF-3 catalyst.

The dependence of OER activity of the F-BSCF catalyst on the F content agrees well with the corresponding double layer capacitances (C_{dl}) of the F-BSCF catalysts (Figs. S3–S4). Similar to the trend of OER activity, all the three F-BSCF catalysts exhibited great C_{dl} value compared with BSCF. C_{dl} of F-BSCF-2 is 6.31 m F cm^{-2}, more than 50% higher than that of BSCF. The improved OER activity of F-BSCF-2 can also be corroborated by significantly reduced charge transfer resistance at η_{10} compared to BSCF and IrO_2 catalysts (Fig. S5). As the F content further increased, C_{dl} of the F-BSCF-3 catalyst was significantly decreased to 4.88 m F cm^{-2} due to the digestion of active oxygen by the excessive F anions. The temperature programmed desorption (TPD) analysis was also investigated (Fig. 3b). Evidently, the desorption temperature of oxygen adsorbed on catalyst surface was substantially reduced with the increase of incorporating F content, and reached the minimum value of approximately 309 °C for F-BSCF-2, which is dramatically down-shifted by 109 °C as compared to that of BSCF, indicating the exceptional O_2 desorption capability of F-BSCF-2 [55,56]. Further increase of the doping F amount results in an up-shifted desorption peak, in good line with the OER performance and DFT calculation results.

In order to further experimentally elucidate the function of the substituted F anion and clarify the process of highly active O^{2-}/O^{-} generation and digestion in-depth as a proof of concept, XPS analysis was carried out (Fig. 4 and Fig. S6). It is clearly revealed by the XPS survey scan spectra of the F-BSCF catalysts (Fig. S6) that F has been successfully introduced to all the three F-BSCF catalysts. The atomic ratio of F in the catalyst is calculated to be 0.98%, 1.90% and 3.10% for

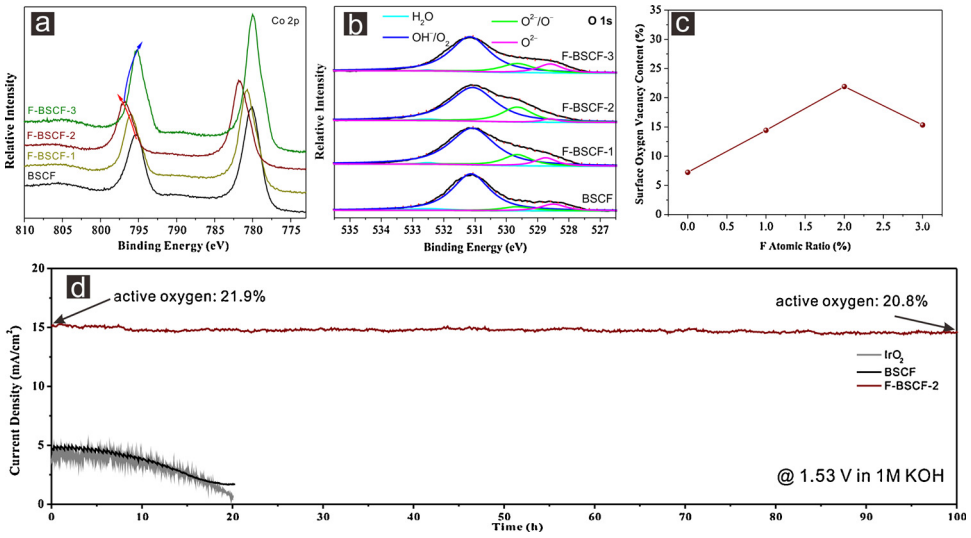

Fig. 4. High resolution (a) Co 2p and (b) O 1s XPS spectra of the F-BSCF catalysts and the pristine BSCF catalyst; (c) Dependence of surface oxygen vancancy content on F content in the F-BSCF catalysts. (d) Time dependence of OER current density at the overpotential of 0.3 V of the F-BSCF-2 catalyst and the IrO_2 catalyst in 1 M KOH.

F-BSCF-1, F-BSCF-2 and F-BSCF-3, respectively, close to the designaion. As expected, the location positions of Co 2*p* peaks of the F-BSCF catalysts are significantly shifted compared with that of BSCF as demonstrated in Fig. 4a. The Co $2p_{1/2}$ peak of F-BSCF-1 at 795.4 eV was positively shifted to 796.0 eV accompanied by the emergence of large numbers of reduced Co oxidation state Co^{2+}, indicating the considerable decrease on the valence of surface Co cations. Meanwhile, the dramatically enhanced concentration of O^{2-}/O^{-} specie was synchronously observed on F-BSCF-1 as depicted in Fig. 4b as a result of the charge compensation for the reduced Co metal ions derived from the oxygen anion partial substitution by fluorine anion. Concretely, the O^{2-}/O^{-} content can be easily doubled from 7.23% of BSCF to 14.42% of F-BSCF-1 (Fig. 4c and Table S4) due to the easier formation of bulk oxygen vacancy, agreeing well with the DFT calculation. For F-BSCF-2, the Co 2*p* peaks are further positively shifted by 1.0 eV, indicating that more Co^{2+} were generated. Correspondingly, F-BSCF-2 exhibited the highest active oxygen content (21.92%), which is the direct reason of its greatest OER activitys. Too much F substitution in BSCF would lead to the regression of Co oxidation state and digestion of O^{2-}/O^{-} as predicted. According to the XPS spectrum of F-BSCF-3, the Co 2*p* peaks are significantly negatively shifted compared with F-BSCF-2, indicating the enhancement on the valence of the Co cations. Accordingly, amount of highly oxidative O^{2-}/O^{-} in the F-BSCF-3 is strongly decreased. The proposed evolution mechanism of O^{2-}/O^{-} was also convincingly proved by the initially decreased and then increased valence state of iron (Fig. S7).

Stability of the extra oxygen active sites in BSCF was confirmed by the long-term durability analysis of the OER activity on F-BSCF-2 (Fig. 4d). There is nearly no current density dereament during the 100 h continuous OER operation at 0.3 V overpotential in 1 M KOH solution. No significant change was observed for the XPS signals from either Co (Fe) or O species (Fig. S8). The highly oxidative O^{2-}/O^{-} in the catalyst was only slightly decreased from 21.9% to 20.8% after 100 h contineous operation. Notably, the OH^{-}/O_2 correspondingly increased from 73.7% to 75.1%, which suggests that the existence of abundant O^{2-}/O^{-} are favorable to the formation of a highly OER-active oxy (hydroxide) surface layer. This was also confirmed by the more rough Fe 2p XPS spectra of the F-BSCF-2 catalyst after the 100 h chronoamperometry test compared to the fresh one. In contrast, OER current density on the IrO_2 and pristine BSCF catalysts were dramatically decreased by ca. 90% from 4.0 mA cm^{-2} to ca. 0.5 mA cm^{-2} and ca. 65% from 4.9 mA cm^{-2} to ca. 1.7 mA cm^{-2}, respectively, during the 20 h operation. Moreover, no OER activity decay was detected after 3000 CV cycling in 1 M KOH solution (Fig. S9). In contrast, OER overpotential at 50 mA cm^{-2} on the commercial IrO_2 catalyst increased by 43 mV.

3. Conclusions

In summary, we proposed a novel strategy to modify the perovskite oxide electrocatalyst with partial F^{-} substitution for further improved OER catalysis activity. The F^{-} in BSCF perovskite lattice would lower the oxidation state of Co(III) and Fe(III) and incurred the surface oxygen anion to highly activated oxidative O^{2-}/O^{-} specie as a consequence of charge compensation. O^{2-}/O^{-} can serve as highly active OER catalytic sites under alkaline condition. With optimized amounts F introduced, the F-BSCF catalyst exhibited extraordinary electrochemical catalytic activity toward OER, requiring an overpotential of merely 280 mV to deliver 10 mA cm^{-2} OER in 1 M KOH. Moreover, the F-BSCF catalyst displayed a proliferated chronoamperometric durability during 100 h continuous OER operation and much superior cycling stability with inappreciable overpotential loss after 3000-cycle CV examination to that of commercial IrO_2. These performances are all among the best-reported oxide based OER catalysts, indicating great potential of F^{-} substitution as a facile and effective strategy for electrocatalyst design.

4. Methods

4.1. Preparations of F-BSCF

To prepare F-BSCF electrocatalyst, 2.6134 g of $Ba(NO_3)_2$ (0.01 mol), 2.1163 g of $Sr(NO_3)_2$ (0.01 mol), 4.6565 g of $Co(NO_3)_2{\cdot}6H_2O$ (0.016 mol) and 1.6160 g of $Fe(NO_3)_3{\cdot}9H_2O$ (0.004 mol) purchased from Sigma-Aldrich with purities higher than 99.97% were dissolved in 35 mL of deionized water under magnetic stirring. After complete dissolution of metal nitrates, a combination of citric acid (0.04 mol, 99.8%, Alfa Aesa) and ethylene diamine tetraacetic acid (EDTA) (0.04 mol, 99.5%, Alfa Aesa) served as complexing agents as well as various contents i.e. 1 mmol, 2 mmol and 3 mmol, respectively, of NH_4F were then added under vigorous stirring for 6 h to form a violet dispersion. Afterwards, the suspension was transferred to a 50 mL of Teflon-lined autoclave, where it was submitted to hydrothermal treatment at 160 °C for 10 h. The derived gel was dried at 60 °C overnight and subsequently annealed at 900 °C for 2 h at a heating rate of 2 °C min^{-1} under ambient atmosphere to obtain the final F-BSCF-x catalysts, where x denotes the designed amount of fluorine source (in mmol) used for the synthesis. For the fabrication of pure BSCF powder, the same procedure was followed except without the addition of ammonium fluoride.

Details on physical characterizations, electrochemical measurements and Density functional theory calculations are provided in

Supporting Information.

Conflict of interest

Nothing declared.

Acknowledgments

We are grateful for financial support from the National Natural Science Foundation of China (Nos. 21875224, 21703211, 21503197 and 21703212) and Natural Science Foundation of Shandong Province (No. ZR2019PEM003).

Appendix A. Supplementary data

Supplementary material related to this article can be found, in the online version, at doi:https://doi.org/10.1016/j.apcatb.2019.117817.

References

[1] J. Xie, H. Zhang, S. Li, R. Wang, X. Sun, M. Zhou, J. Zhou, X.W. Lou, Y. Xie, Adv. Mater. 25 (2013) 5807–5813.
[2] J. Zhang, T. Wang, P. Liu, Z. Liao, S. Liu, X. Zhuang, M. Chen, E. Zschech, X. Feng, Nat. Commun. 8 (2017) 15437.
[3] J. Xiong, J. Li, J. Shi, X. Zhang, N.-T. Suen, Z. Liu, Y. Huang, G. Xu, W. Cai, X. Lei, L. Feng, Z. Yang, L. Huang, H. Cheng, ACS Energy Lett. 3 (2018) 341–348.
[4] J. Wang, M. Yan, K. Zhao, X. Liao, P. Wang, X. Pan, W. Yang, L. Mai, Adv. Mater. 29 (2017) 1604464–1614469.
[5] H.B. Wu, B.Y. Xia, L. Yu, X.-Y. Yu, X.W. Lou, Nat. Commun. 6 (2015) 6512.
[6] X. Xu, Y. Chen, W. Zhou, Z. Zhu, C. Su, M. Liu, Z. Shao, Adv. Mater. 28 (2016) 6442–6448.
[7] Y. Lyu, R. Wang, L. Tao, Y. Zou, H. Zhou, T. Liu, Y. Zhou, J. Huo, S.P. Jiang, J. Zheng, S. Wang, Appl. Catal. B: Environ. 248 (2019) 277–285.
[8] W. Yanyong, X. Chao, Z. Zhiyuan, L. Dongdong, C. Ru, W. Shuangyin, Adv. Funct. Mater. 28 (2018) 1703363.
[9] S. She, J. Yu, W. Tang, Y. Zhu, Y. Chen, J. Sunarso, W. Zhou, Z. Shao, ACS Appl. Mater. Inter. 10 (2018) 11715–11721.
[10] L. Xien, P. Minjoon, K.M. Gyu, G. Shiva, W. Gang, C. Jaephil, Angew. Chem. Int. Ed. 54 (2015) 9654–9658.
[11] G. Wu, A. Santandreu, W. Kellogg, S. Gupta, O. Ogoke, H. Zhang, H.-L. Wang, L. Dai, Nano Energy 29 (2016) 83–110.
[12] Z. Liu, Y. Wang, R. Chen, C. Chen, H. Yang, J. Ma, Y. Li, S. Wang, J. Power Sources 403 (2018) 90–96.
[13] Y. Zeng, L. Chen, R. Chen, Y. Wang, C. Xie, L. Tao, L. Huang, S. Wang, J. Mater. Chem. A 6 (2018) 24311–24316.
[14] X. Xu, Y. Chen, W. Zhou, Y. Zhong, D. Guan, Z. Shao, Adv. Mater. Interfaces 5 (2018) 1701693.
[15] I.C. Man, H.Y. Su, F. Calle-Vallejo, H.A. Hansen, J.I. Martínez, N.G. Inoglu, J. Kitchin, T.F. Jaramillo, J.K. Nørskov, J. Rossmeisl, ChemCatChem 3 (2011) 1159–1165.
[16] J. Rossmeisl, Z.-W. Qu, H. Zhu, G.-J. Kroes, J.K. Nørskov, J. Electroanal. Chem. 607 (2007) 83–89.
[17] F. Lyu, Y. Bai, Z. Li, W. Xu, Q. Wang, J. Mao, L. Wang, X. Zhang, Y. Yin, Adv. Funct. Mater. 27 (2017) 1702324.
[18] Y. Zhu, W. Zhou, Z.-G. Chen, Y. Chen, C. Su, M.O. Tadé, Z. Shao, Angew. Chem. Int. Ed. 54 (2015) 3897–3901.
[19] G. Shiva, K. William, X. Hui, L. Xien, C. Jaephil, W. Gang, Chem. Asian J. 11 (2016) 10–21.
[20] X. Xu, Y. Pan, W. Zhou, Y. Chen, Z. Zhang, Z. Shao, Electrochim. Acta 219 (2016) 553–559.
[21] C. Su, W. Wang, Y. Chen, G. Yang, X. Xu, M.O. Tadé, Z. Shao, ACS Appl. Mater. Inter. 7 (2015) 17663–17670.
[22] X. Xu, W. Wang, W. Zhou, Z. Shao, Small Methods 2 (2018) 1800071.
[23] F. Cheng, T. Zhang, Y. Zhang, J. Du, X. Han, J. Chen, Angew. Chem. Int. Ed. 52 (2013) 2474–2477.
[24] L. Xu, Q. Jiang, Z. Xiao, X. Li, J. Huo, S. Wang, L. Dai, Angew. Chem. Int. Ed. 128 (2016) 5363–5367.
[25] Y. Wang, T. Zhou, K. Jiang, P. Da, Z. Peng, J. Tang, B. Kong, W.B. Cai, Z. Yang, G. Zheng, Adv. Energy Mater. 4 (2014) 1400696.
[26] G. Huang, Z. Xiao, R. Chen, S. Wang, ACS Sustain. Chem. Eng. 6 (2018) 15954–15969.
[27] R. Zhang, Y.-C. Zhang, L. Pan, G.-Q. Shen, N. Mahmood, Y.-H. Ma, Y. Shi, W. Jia, L. Wang, X. Zhang, W. Xu, J.-J. Zou, ACS Catal. (2018) 3803–3811.
[28] J. Huang, J. Han, R. Wang, Y. Zhang, X. Wang, X. Zhang, Z. Zhang, Y. Zhang, B. Song, S. Jin, ACS Energy Lett. 3 (2018) 1698–1707.
[29] X. Xu, C. Su, W. Zhou, Y. Zhu, Y. Chen, Z. Shao, Adv. Sci. 3 (2016) 1500187.
[30] X. Pan, M.Q. Yang, X. Fu, N. Zhang, Y.J. Xu, Nanoscale 5 (2013) 3601–3614.
[31] J. Suntivich, K.J. May, H.A. Gasteiger, J.B. Goodenough, Y. Shao-Horn, Science 334 (2011) 1383–1385.
[32] J. Suntivich, H.A. Gasteiger, N. Yabuuchi, H. Nakanishi, J.B. Goodenough, Y. Shao-Horn, Nat. Chem. 3 (2011) 546–550.
[33] W.G. Hardin, J.T. Mefford, D.A. Slanac, B.B. Patel, X. Wang, S. Dai, X. Zhao, R.S. Ruoff, K.P. Johnston, K.J. Stevenson, Chem. Mater. 26 (2014) 3368–3376.
[34] Y. Tong, Y. Guo, P. Chen, H. Liu, M. Zhang, L. Zhang, W. Yan, W. Chu, C. Wu, Y. Xie, Chem 3 (2017) 812–821.
[35] E. Fabbri, M. Nachtegaal, X. Cheng, T.J. Schmidt, Adv. Energy Mater. 5 (2015) 1402033.
[36] C.T. Alexander, A.M. Abakumov, R.P. Forslund, K.P. Johnston, K.J. Stevenson, ACS Appl. Energy Mater. (2018).
[37] J. Kim, X. Yin, K.-C. Tsao, S. Fang, H. Yang, J. Am. Chem. Soc. 136 (2014) 14646–14649.
[38] C.-F. Chen, G. King, R.M. Dickerson, P.A. Papin, S. Gupta, W.R. Kellogg, G. Wu, Nano Energy 13 (2015) 423–432.
[39] Z. Zhenbao, Z. Yinlong, Z. Yijun, Z. Wei, S. Zongping, Adv. Energy Mater. 7 (2017) 1700242.
[40] Y. Li, Y. Li, Y. Wan, Y. Xie, J. Zhu, H. Pan, X. Zheng, C. Xia, Adv. Energy Mater. 9 (2019) 1803156.
[41] J. Zhu, G. Liu, Z. Liu, Z. Chu, W. Jin, N. Xu, Adv. Mater. 28 (2016) 3511–3515.
[42] B. Hua, M. Li, W. Pang, W. Tang, S. Zhao, Z. Jin, Y. Zeng, B. Shalchi Amirkhiz, J.-L. Luo, Chemistry 4 (2018) 2902–2916.
[43] Z. Shao, S.M. Haile, Nature 431 (2004) 170.
[44] Y. Duan, S. Sun, S. Xi, X. Ren, Y. Zhou, G. Zhang, H. Yang, Y. Du, Z.J. Xu, Chem. Mater. 29 (2017) 10534–10541.
[45] H. Liang, Y. Hong, C. Zhu, S. Li, Y. Chen, Z. Liu, D. Ye, Catal. Today 201 (2013) 98–102.
[46] T. Soga, K. Ohwada, M. Iwasaki, J. Chem. Phys. 61 (1974) 1990–1995.
[47] J.-I. Jung, H.Y. Jeong, J.-S. Lee, M.G. Kim, J. Cho, Angew. Chem. 126 (2014) 4670–4674.
[48] L. Hang, Y. Sun, D. Men, S. Liu, Q. Zhao, W. Cai, Y. Li, J. Mater. Chem. A 5 (2017) 11163–11170.
[49] Z. Xiao, Y. Wang, Y.-C. Huang, Z. Wei, C.-L. Dong, J. Ma, S. Shen, Y. Li, S. Wang, Energy Environ. Sci. 10 (2017) 2563–2569.
[50] L. Trotochaud, J.K. Ranney, K.N. Williams, S.W. Boettcher, J. Am. Chem. Soc. 134 (2012) 17253–17261.
[51] H. Hu, B. Guan, B. Xia, X.W. Lou, J. Am. Chem. Soc. 137 (2015) 5590–5595.
[52] T. Ling, D.-Y. Yan, Y. Jiao, H. Wang, Y. Zheng, X. Zheng, J. Mao, X.-W. Du, Z. Hu, M. Jaroniec, S.-Z. Qiao, Nat. Commun. 7 (2016) 12876.
[53] X. Li, J. Zhang, Q. Feng, C. Pu, L. Zhang, M. Hu, X. Zhou, X. Zhong, W. Yi, J. Tang, Z. Li, X. Zhao, H. Li, B. Xu, J. Mater. Chem. A 6 (2018) 17288–17296.
[54] E. Omari, M. Omari, D. Barkat, Polyhedron 156 (2018) 116–122.
[55] S. Lu, J. Pan, A. Huang, L. Zhuang, J. Lu, Proc. Natl. Acad. Sci. 105 (2008) 20611–20614.
[56] L. Peng, J. Wang, Y. Nie, K. Xiong, Y. Wang, L. Zhang, K. Chen, W. Ding, L. Li, Z. Wei, ACS Catal. (2017) 8184–8191.